



Investigation of hybrid CuPc-doped ZnO/p-silicon photodiodes for photonic and electronic applications

Gökhan Özel¹ and Selçuk Demirezen^{2,*}

¹ Institute of Science, Renewable Energy and Application Programme, Amasya University, Amasya, Turkey

² Sabuncuoğlu Şerefeddin Vocational School of Health Services, Amasya University, Amasya, Turkey

Received: 25 November 2023

Accepted: 27 April 2024

© The Author(s), 2024

ABSTRACT

Copper phthalocyanine (CuPc) doped zinc oxide (ZnO) interlayered Al/p-Si Schottky barrier diodes (SBDs) were systematically fabricated utilizing spin coating technique. This study was undertaken to meticulously assess the influence of varying concentrations of CuPc on the intricate electrical and photodiode characteristics of these devices. The investigation involved the characterization of the current–voltage (I – V) characteristics configured with distinct different doping concentrations of CuPc such as 0.05 wt%, 1 wt%, 2 wt%, under a wide range of voltages (± 5 V) and illumination irradiances. These measurements enabled the calculation of various critical electrical variables, such as the ideality factor (n), barrier height (Φ_B), series resistance (R_s), shunt resistance (R_{sh}), interface states density (N_{ss}) and their response under various illumination levels (between 10 and 100 mW/cm²) and under dark condition. An increase in the reverse current as the illumination increases suggested the potential utility of these SBDs as photodiodes, photosensors, or photodetectors. Notably, the linear dynamic range (LDR), a crucial factor for image sensors which obtained around 14 for all photodiodes. The photodiodes exhibited a good rectification ratio (RR) of approximately 10^4 . The results obtained indicate that the rectifying properties of the structures can be controlled by CuPc doping. In addition, the results indicated that the presence of CuPc significantly influenced the values of n , Φ_B , R_s/R_{sh} , and N_{ss} . To further analyze the devices, capacitance–voltage (C – V) and conductance–voltage (G – V) measurements were carried out to determine parameters such as diffusion potential (V_D), dopant acceptor atoms concentration (N_A), Fermi energy level (E_F), and width of depletion layer (W_D) at both 1 kHz and 1 MHz. The measurements revealed that the capacitance values were higher at low frequencies compared to high frequencies, and this behavior was attributed to N_{ss} . In summary, this study suggests that the manufactured photodiodes have the potential to be employed as photodiodes, sensors, or detectors in optical sensing applications, and their performance can be tailored by adjusting the concentration of CuPc in the ZnO

Address correspondence to E-mail: selcukdemirezen@gmail.com

<https://doi.org/10.1007/s10854-024-12677-3>

Published online: 12 May 2024

Springer

interlayered structures. The discerned outcomes revealed the substantial influence of CuPc concentration on key electrical parameters, with conspicuous trends noted in the values of n , Φ_B , R_s/R_{sh} and N_{ss} . Furthermore, the observed increase in the reverse current as the illumination level increases highlights the potential utility of these SBDs as sensitive photodiodes/sensors/detectors.

1 Introduction

Schottky barrier diodes (SBDs) or Schottky diodes (SD), which is formed by the junction of a metal with a semiconductor and designed using the Schottky effect, which creates a barrier to the flow of electrons at the metal–semiconductor junction, have gained paramount significance in the realm of technology, owing to their diverse applications encompassing photodiodes, solar cells, radio frequency detectors, and transistors [1–6]. Moreover, by customizing the materials employed in their fabrication, such as by adding a thin insulating layer between the metal and the semiconductor for convert it to metal/insulator/semiconductor (MIS), metal/polymer/semiconductor (MPY) or metal/ferroelectric/semiconductor (MFS) structures, we can unlock the incredible potential of Schottky diodes in the realm of photodetectors. To vary and manage the barrier height, an organic/inorganic semiconducting or insulating interlayer can be used, therefore, it is crucial to determine the electrical characteristics of metal/interlayer/semiconductor devices [1, 7]. These interfaces wield substantial influence over critical Schottky barrier attributes, including barrier height (Φ_B), ideality factor (n), and series resistance (R_s). Optimizing these parameters, along with achieving the highest rectification ratio ($RR = I_F/I_R$), shunt resistance (R_{sh}) and minimizing leakage current, R_s , and surface states (N_{ss}), hinges significantly on the dielectric constant of the interface material chosen [8–12]. Consequently, the electrical characteristics delineated above assume paramount importance in the comprehensive analysis of structure and crucial for optimizing and designing devices for applications such as photodetectors, solar cells, and light-emitting diodes, where the interaction between light and semiconductors plays a central role in their operation. On the other hand, the importance of photodiodes in this field has grown considerably, thanks to advances in semiconductor technology and the emergence of new-generation materials. Known for their high sensitivity to photons and high-energy particles, photodiodes operate effectively under

reverse bias conditions, converting light into electrical current. When incident light with energy greater than the bandgap of the semiconductor hits the photodiode, it creates electron–hole pairs. The electric field in the junction then facilitates the separation of the charges, directing them towards the neutral region and preventing electron–hole recombination. This process results in the generation of a photocurrent, which leads to the production of an electrical signal. Notably, the photo-response of the device is more pronounced in the reverse bias region than in the forward bias region. The variation in photocurrent was studied by manipulating the illumination intensity under reverse bias conditions [13–15].

ZnO exhibits excellent electron mobility, with values typically exceeding $100 \text{ cm}^2/\text{V s}$ [16, 17]. The wide exciton binding energy facilitates the generation of robust near-band-edge excitonic emissions at both room temperature and elevated temperatures. ZnO boasts a direct wide bandgap of approximately 3.37 eV at 300 K, allowing it to detect ultraviolet (UV) light with wavelengths down to 370 nm [18]. In addition, ZnO have low dark current, rapidly respond to changes in incident light intensity (order of microseconds to milliseconds), robust and can withstand environmental factors, relatively cost-effective to produce, bio-safe, bio-compatible and environmental-friendly [16–19]. Therefore, ZnO's exceptional properties make it an attractive choice for photodiodes, offering high sensitivity, fast response times, and versatility across a wide range of wavelengths while maintaining cost-effectiveness and durability. On the other hand, utilizing zinc oxide (ZnO) as an interface material in p-Si Schottky barrier diodes (SBDs) presents a myriad of significant advantages over their counterparts fabricated without interface layers. Benhaliliba [20] examined and clearly described the conduction mechanisms for ZnO/p-Si heterojunctions using the average of current–voltage, capacitance, and conductance vs voltage profiles, and found decreasing Schottky effect in the metal–insulator energy barrier as a result of electrostatic interaction with the electric field at a

metal–insulator interface. Rajan et al. [21] have fabricated Au/ZnO/n-Si Schottky diodes and investigated its electrical characteristics through I – V and C – V characterizations. They reported the rectifying nature of the diode, with rectifying ratio of 93, ideality factor of ~ 6 , barrier height of 0.804 eV and saturation current of 1.37×10^{-10} A. Aydoğan et al. [22] used electro-deposition technique to fabricate Au/n-ZnO/n-Si Schottky diodes for investigated its electrical characteristics and reported the values of ideality factor, barrier height and rectification ratio as 1.21, 0.61 eV, and 3×10^4 .

Organic materials, endowed with attributes such as cost-effectiveness, flexibility, ease of production, and adaptability to large-scale applications, have spurred heightened interest in leveraging them for the creation of organic-based electronic and optoelectronic devices. Studies have shown that, organic-based semiconductors have enormous properties such as reduced environmental footprint, lower energy consumption, resource conservation, biodegradability, versatility and adaptability, recyclability, reduction of hazardous chemicals, improved energy harvesting, in addition, may simplify the recycling and disposal of electronic waste, which is a growing environmental concern. Considerable interest has been directed toward the incorporation of organic materials in electronic devices owing to its distinct characteristics and prospective practices. Phthalocyanines (Pc) are chemically and thermally stable, and the π -system consisting of 18 π electrons in the macrosilicic ring has light absorption sensitivity in a visible region (400–700 nm) and when incorporate different metals into center named as metallophthalocyanine [23, 24]. Among them, copper phthalocyanine (CuPc) has shown great promise as an interface material in Schottky diodes. CuPc is an organic semiconductor that exhibits excellent charge transport properties, high thermal stability, and a well-defined energy level structure. CuPc has been successfully employed in organic photovoltaics (OPVs) as an interface material in Schottky diodes. Although there have been a number of attempts to produce hybrid composite films, there have been only a few attempts, in particular on the formation of metal-phthalocyanine composite hybrid materials. Wang et al. [25] formed Ni-doped CuPc films on indium tin oxide substrates and carried out structural analysis. They found that the films had flat surface morphology and that the CuPc films retained their initial amorphous phase, showing only changes in crystallite sizes or crystallinity and modification of

carrier transport with increasing Ni doping levels. Reddy et al. [26] fabricated organic–inorganic hybrid composite interlayers such as Au-CuPc films with various Au and CuPc compositions for Al/n-type Si SBDs at room temperature, and found that the Φ_{B0} , n and R_s values of Al/n-type Si SBDs with Au-CuPc interlayer decreased with increasing Au content. Tatar et al. [27] fabricated an organic–inorganic hybrid Ag/p-CuPc/a-Si/n-Si/Ag and Ag/p-CuPc/a-Si/p-Si/Ag heterojunction photovoltaic devices using chemical spray pyrolysis technique. They found that the electrical and morphological properties of p-CuPc/a-Si/c-Si hybrid heterojunction photovoltaic devices are very promising for device performance, stability and reliability.

In this research endeavor, we employed a ZnO with doped varying percentages of CuPc (0.05%, 0.10%, and 0.20%) interlayer at the Al/p-Si (metal/semiconductor) interface to assess its suitability as a potential candidate for modifying the behavior of charge carriers at this interface. Our primary objective was to investigate the contribution of the CuPc-doped ZnO thin film to the photoconductive and electronic properties, including Φ_B , n , reverse saturation current (I_0), N_{ss} , RR, and R_s , within Au/n-Si type Schottky diodes. This research looked at current–voltage (I – V) characteristics as well as capacitance/conductance (C/G – V) characteristics. A thorough exploration of the impact of these interfacial layers on the electrical and photoconduction characteristics of these devices was conducted, involving extensive I – V measurements under different illumination conditions and over various time intervals. Additionally, C/G – V measurements were carried out with frequency dependence analysis over a wide voltage/frequency range, providing a detailed and comprehensive assessment of the interface's influence on device performance. The experimental outcomes demonstrate a notable enhancement in device performance when utilizing a 0.10% CuPc–ZnO interlayer. This enhancement is characterized by a heightened RR value and concurrently lower N_{ss} and R_s values.

2 Experimental procedure

A CuPc-doped ZnO material with varying CuPc ratios was synthesized through the sol–gel method and deposited as thin films onto p-type Silicon (Si) substrates. The Silicon substrates had a thickness of 600 μm , a resistivity of 5–10 Ω cm, and a $\langle 111 \rangle$ orientation. Initially, zinc acetate

dihydrate $[\text{Zn}(\text{CH}_3\text{COO})_2 \cdot 2\text{H}_2\text{O}]$ was employed as the source of zinc. Additionally, 2-methoxyethanol ($\text{CH}_3\text{OCH}_2\text{-CH}_2\text{OH}$) served as the solvent, while monoethanolamine $[\text{NH}_2\text{CH}_2\text{CH}_2\text{OH}]$ acted as a stabilizer. The solutions of Cu phthalocyanine were separately prepared in dimethylformamide ($\text{DMF}:(\text{CH}_3)_2\text{NC}(\text{O})\text{H}$). A p-type Si wafer had aluminum (Al) metal evaporated on its backside using a thermal evaporation system. Subsequently, the p-Si/Al contact underwent thermal treatment at 550°C for 5 min in a nitrogen (N_2) atmosphere to reduce resistance. The CuPc-doped ZnO materials were then synthesized in various amounts [0.05 wt.%, 0.1 wt.%, and 0.2 wt.%]. The resultant mixes were blended for 3 h at 70°C to ensure they were homogenous and transparent. The finished solutions were allowed to stabilise at room temperature for 24 h after this procedure and before coating onto silicon. Once the interlayer materials were ready, they were applied onto the silicon substrate using spin coating at 2000 rpm, which had been chemically cleaned and connected to aluminum to form ohmic contacts. The coating duration was set at 8 s. Using a shadow mask, aluminium rectifier contacts with a radius of 0.5 mm were created on the film-coated substrates. Figure 1 shows a schematic depiction of the produced devices. A Fytronix 9000 Solar I - V / C - V characterization system was used to evaluate the electrical properties of the Al/CuPc:ZnO/p-Si photodiodes. An AA class solar simulator, a source meter, and a C - V analyzer were incorporated in this system. The diode's photoelectric performance was investigated under various lighting situations.

3 Results and discussion

3.1 Optoelectronic features

It is also of interest to explore the influence of factors such as illumination intensity, operating frequency, and applied voltage on the I - V and C / G - V characteristics in both reverse and forward bias configurations. MS architectures that incorporate a thin insulating layer, whether it be oxide or polymer (organic or inorganic), at the interface between the metal and semiconductor can exhibit heightened sensitivity to light, particularly within the reverse bias region. When the energy of incident photons exceeds the semiconductor's bandgap (E_g), a significant quantity of electron-hole pairs can be produced in the vicinity of the mid-gap. In the case of Al/CuPc:ZnO/p-Si photodiodes, various CuPc concentrations (0.05, 0.10, and 0.20 wt%) were employed, and their forward and reverse bias I - V characteristics were examined under both dark and illuminated conditions. The results are depicted in Fig. 2a-c.

In these presented figures (Fig. 2a-c), it is evident that the photo current (I_{ph}) notably increases as the illumination intensity rises, particularly within the reverse bias region. This phenomenon can be attributed to the higher electric field strength in the reverse bias region as compared to the forward bias region within each diode. The augmentation of reverse bias current results from the generation of electron-hole pairs induced by the illumination effect. In simpler terms, a substantial number of electron-hole pairs are generated when exposed to light, giving rise to a photoconductive behavior. This behavior can be elucidated by the fact that electrons in the valence band

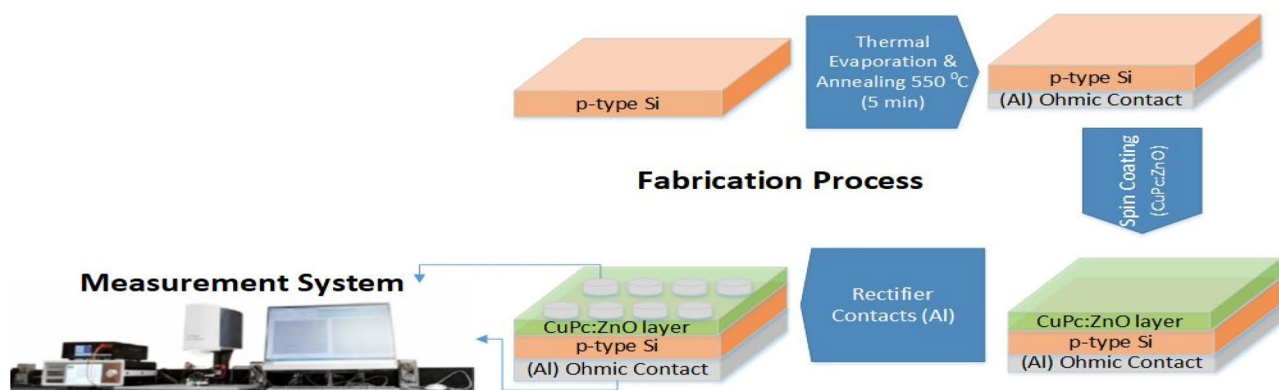


Fig. 1 A schematic diagram for the characterisation of electrical devices

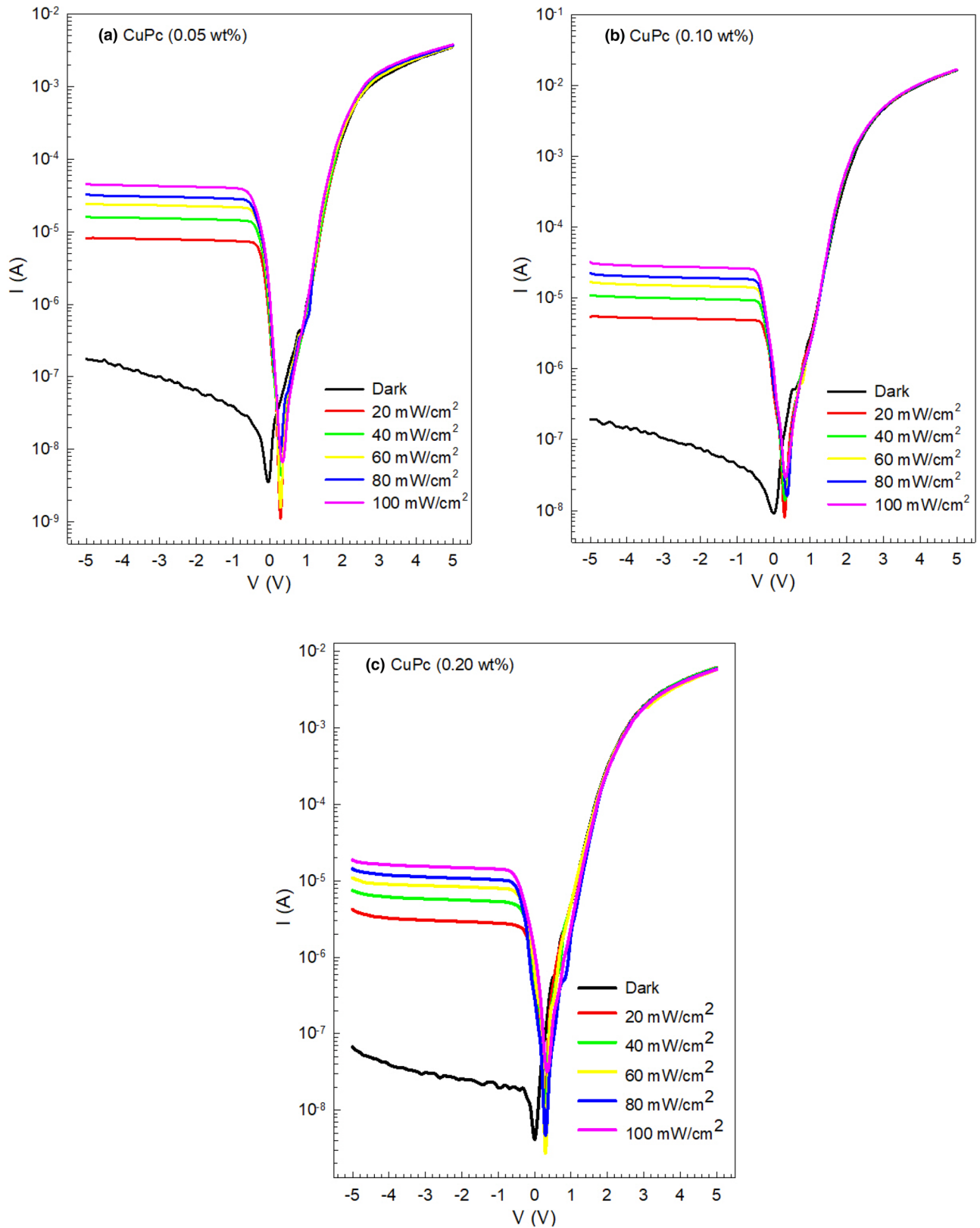


Fig. 2 I - V plots of Al/CuPc:ZnO/p-Si photodiodes under different CuPc concentration levels, with measurements conducted in both dark and illuminated conditions

absorb sufficient energy ($hc/q\lambda \geq E_g$) to transition into the conduction band. While the recombination of electron–hole pairs encounters hindrance under the influence of a high electric field in the reverse bias region, they tend to recombine more readily in the forward bias region due to the lower electric field strength present.

Typically, the photoconductive behavior can be characterized using the following equation:

$$I_{\text{ph}} = AP^m \quad (1)$$

In this equation, I_{ph} stands for photocurrent, A stands for constant, P stands for illumination intensity,

and m is an exponent linked with illumination intensity. By calculating the logarithm of both sides of Eq. 1, we arrive at:

$$\log I_{\text{ph}} = m \log P + B \quad (2)$$

In Eq. 2, B is equal to $\log A$, and m can be determined from the slope of the linear portion of the $\log(I_{\text{ph}})$ vs. $\log(P)$ plot. Figure 3a illustrates the $\log(I_{\text{ph}})$ vs $\log(P)$ plots for each diode with varying concentrations of CuPc (0.05 wt.%, 0.1 wt.%, and 0.2 wt.%) at -5 V. The m values of 1.03, 1.03, and 0.97 were obtained for photodiodes at these concentrations. The value of m serves as an indicator of the

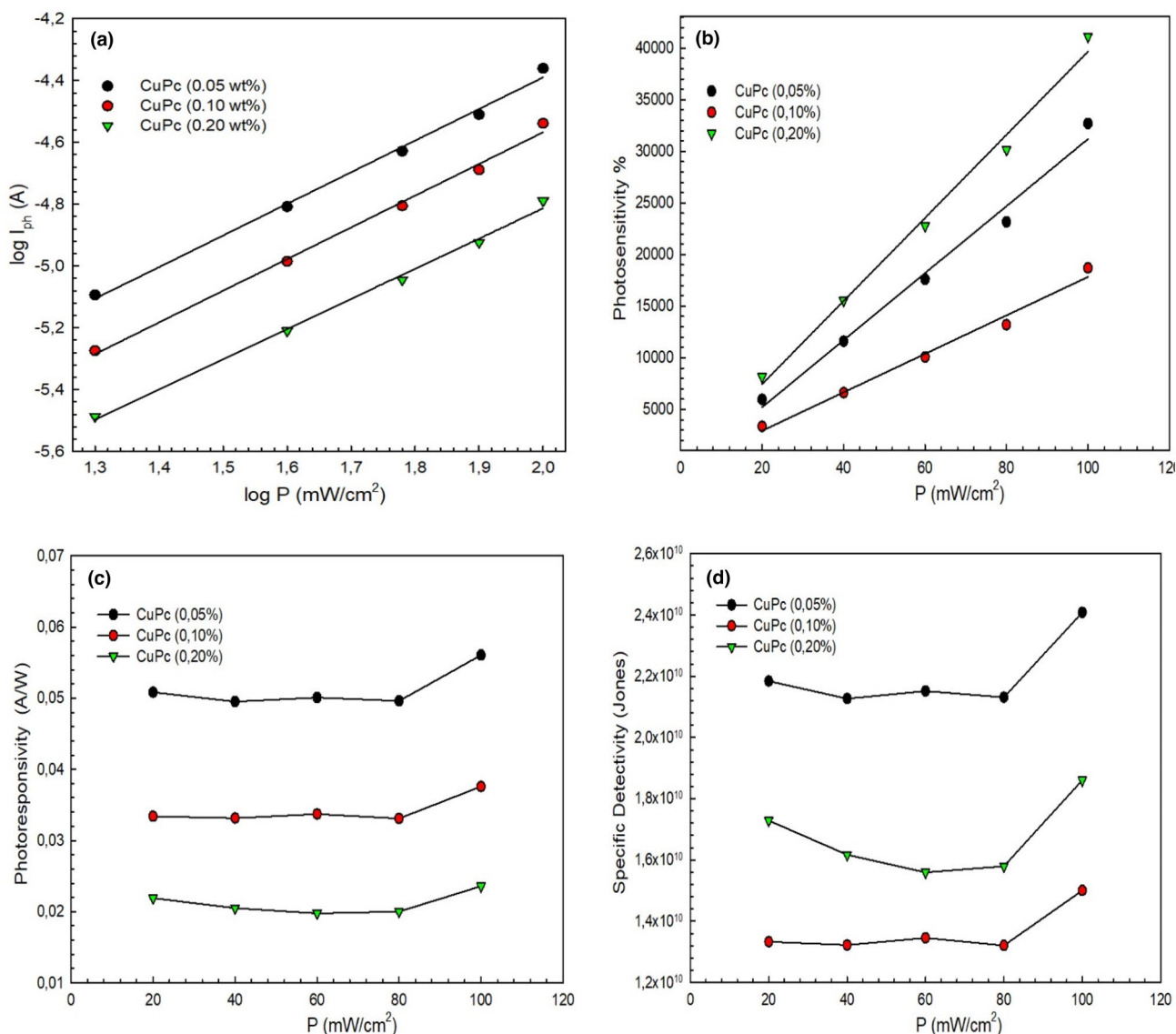


Fig. 3 Illumination and bias dependent parameters for the Al/CuPc:ZnO/p-Si photodiodes

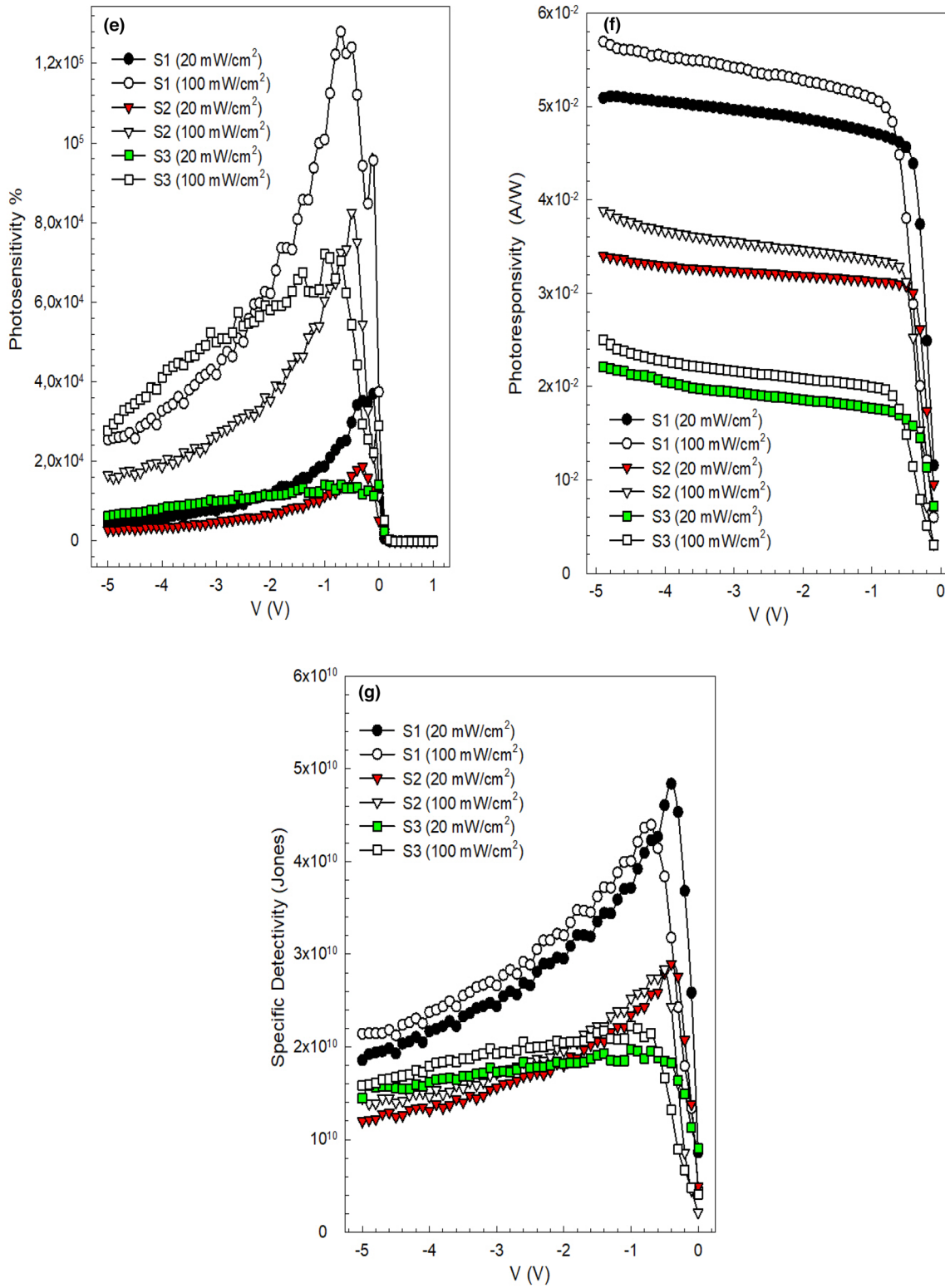


Fig. 3 continued

type of photoconduction mechanism at play in the diode sample. When m falls within the range of 0.5 to 1, the photoconduction process is associated with trap levels. Conversely, if m exceeds 1, the photoconduction mechanism is linked to lower densities of unoccupied trap levels, as documented in previous research [28–31]. Based on the m values observed in this study, it becomes evident that the photocurrent exhibits a linear photoconduction behavior, indicative of the underlying photoconduction process. These findings strongly suggest that Al/CuPc:ZnO/p-Si Schottky barrier diodes have the potential to serve as highly effective photodiodes or photo devices.

A photodetector's linear dynamic range (LDR) is defined as the range over which the photodetector's current response maintains a linear and proportionate correlation with the intensity of the incoming light. This correlation is described as follows:

$$\text{LDR} = 20 \log \left(\frac{J_{\max}}{J_{\min}} \right) \quad (3)$$

where J_{\max} the maximum and J_{\min} minimum observed current densities. In the case of S1, S2, and S3 at -5 V, the LDR values were calculated as 14.65, 14.71, and 13.96, respectively. LDR is crucial for image sensors since they need to function effectively across a broad spectrum of light intensities. To put it simply, having a sufficiently wide LDR is essential to ensure that clear and detailed images can be captured in various lighting conditions [31–33]. According to the this findings, it is evident that Al/CuPc:ZnO/p-Si structures are well-suited for applications as photo devices and image sensors.

Illumination and bias effect on photosensitivity, photoresponsivity and specific detectivity are given in Fig. 3. The equation can be employed to compute the photosensitivity (S) of optoelectronic devices, which is expressed as:

$$S(\%) = \left(\frac{I_{\text{photo}} - I_{\text{dark}}}{I_{\text{dark}}} \right) \times 100 \quad (4)$$

The graph illustrating the relationship between photosensitivity and light intensity is presented in Fig. 3b. As there is a linear correlation between S and I_{phv} the values of S increase in tandem with the rising intensity of incident light. This increase in photosensitivity with increasing light intensity can be attributed to the photoconductive characteristics

of Al/CuPc:ZnO/p-Si SBDs. The results also suggest that it operates in a manner akin to a photodiode. In essence, it can be inferred that the augmentation in the quantity of photogenerated carriers due to the heightened light intensity results in an increase in the photodiode's photocurrent [34].

In addition, the photoresponsivity (R) and the specific detectivity (D^*) are two other important parameters for photodevices, which can be calculated by means of the following equations;

$$R = \frac{I_{\text{photo}} - I_{\text{dark}}}{PA} \quad (5)$$

$$D^* = R \sqrt{\frac{A}{2qI_d}} \quad (6)$$

where q is the elementary charge and A is the active area. High detectivity, as shown in Eq. 6, requires not only high sensitivity (high photocurrent) but also low dark current (low noise). The illuminance dependent R and D^* graphs are shown in Fig. 3. The R and D^* values are strongly dependent on the light intensity as can be seen in these figures. As can be seen from both figures, R and D are higher at higher than lower intensities. In addition, R shows a partial increase with increasing applied voltage. The S1 photosensor's highest R value was about 50 mA/W, decreasing with decreasing bias. All the above illumination characteristics of Al/CuPc:ZnO/p-Si suggest that it can be used as a photodiode.

Thermionic emission (TE) theory application facilitates the assessment of the forward bias I - V characteristics in structures including different CuPc-doped variants, with a particular focus on intermediate bias voltages ($V \geq 3kT/q$). This evaluation will be carried out using the following equations as [1, 2];

$$I = I_o \exp \left(\frac{q(V - IR_s)}{nkT} \right) \quad (7)$$

$$n = \frac{q}{kT} \frac{d(V - IR_s)}{d(\ln(I))} \quad (8)$$

In Eqs. 5 and 6, I_o is the reverse bias saturation current, while n is the ideality factor. These parameters are determined by analyzing the intercept and slope of the linear segment of the $\ln I$ - V at zero bias. The barrier height (Φ_B) is derived from the I_o value as follows:

$$\Phi_{Bo} = \frac{kT}{q} \ln \left(\frac{AA^*T^2}{I_o} \right) \tag{9}$$

"T" is the absolute temperature measured in degrees Kelvin, while "k" is the Boltzmann constant. In addition, "A*" represents the effective Richardson constant, which is 32 A/cm²K² for p-type silicon. In order to evaluate and compare the rectification rate (RR), I_o, and n characteristics of the Al/CuPc:ZnO/p-Si photodiodes with different CuPc contents, the semi-logarithmic forward and reverse bias I–V characteristics are shown in Fig. 4a for dark conditions and in Fig. 4b under an illumination intensity of 100 mW/cm².

The semi-logarithmic I–V plot of the Al/CuPc:ZnO/p-Si photodiodes was studied to evaluate the rectification rate (RR), I_o and n by varying the amount of CuPc used. As shown in Fig. 4, the structures exhibit both photovoltaic and excellent rectifying behavior (at ±5 V, order of 10⁴), resulting in a meaningful reduction in leakage current. The higher content CuPc significantly reduces charge separation in the reverse bias, and in turn the reverse current is significantly reduced, so the reverse current of S3 is less than that of S1 and S2. Table 1 displays the RR = I_F/I_R values for the S1, S2, and S3 which were determined to be 1.9 × 10⁴, 8.6 × 10⁴ and 9.2 × 10⁴ at ±5 V, respectively. It is evident that the structure with 2 wt.% CuPc is more

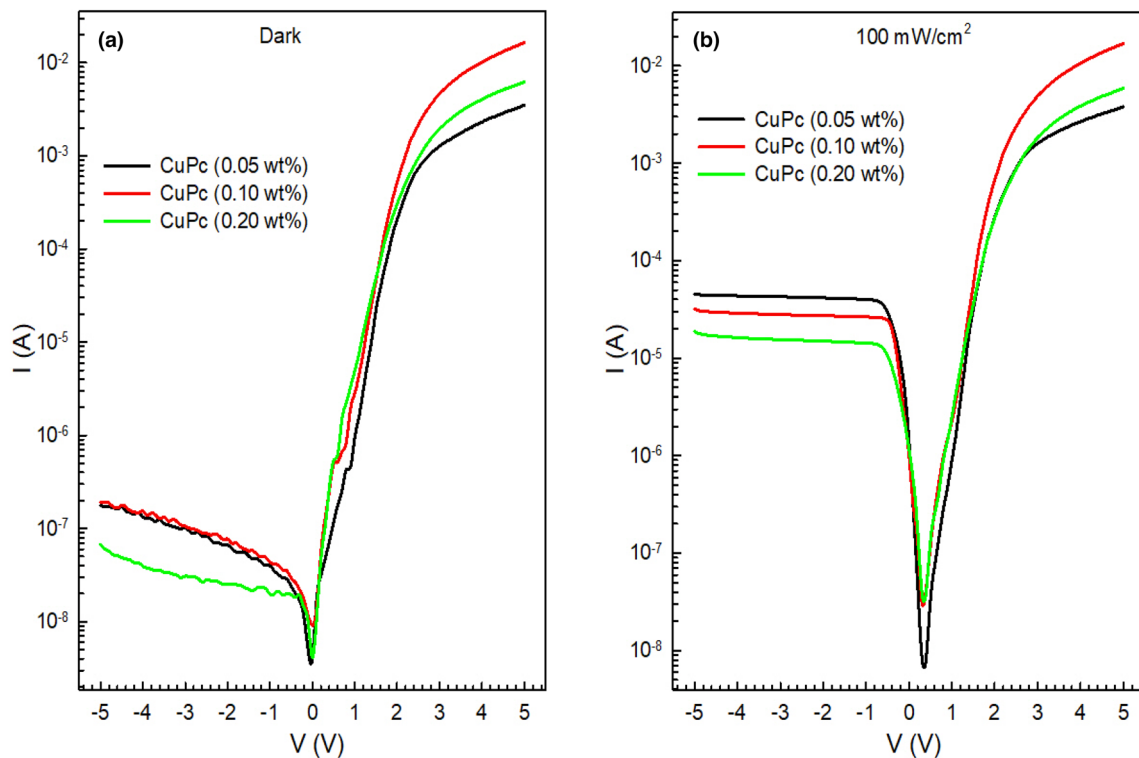


Fig. 4 The I–V characteristics for Al/CuPc:ZnO/p-Si photodiodes **a** for dark conditions **b** under an illumination intensity of 100 mW/cm²

Table 1 The main electrical parameters derived from Al/CuPc:ZnO/p-Si photodiode I–V characteristics

	Dark						Under 100 mW/cm ²					
	RR (× 10 ⁴)	I _o (A) (× 10 ⁻⁹)	n	Φ _B (eV)	R _s (Ω)	R _{sh} (MΩ)	I _o (A) (× 10 ⁻⁹)	n	Φ _{Bo} (eV)	R _s (Ω)	R _{sh} (kΩ)	
S1(0.5 wt%)	1.9	0.11	8.26	0.73	1490	28	0.28	4.95	0.81	1370	106	
S2 (1 wt%)	8.6	7.61	4.45	0.74	319	26	2.06	5.44	0.77	308	156	
S3 (2 wt%)	9.2	5.19	4.01	0.75	836	93	5.60	5.60	0.76	881	273	

rectified. This means that the leakage current of the S3 is considerably reduced compared to the others. Table 2 also presents the I_o , n , and Φ_B values for the Al/CuPc:ZnO/p-Si photodiodes, which were obtained using TE theory under both dark and illuminated conditions (at 100 mW/cm²). As can be seen, Φ_B increase and n decrease with increasing CuPc concentration. Normally, n must be 1 for a diode to be perfect. In practise, however, factors such as semiconductor tunnelling current, N_{ss} spatial density distribution, the existence of barrier inhomogeneities, the interlayer, as well as carrier injection and generation-recombination effects all contribute to n exceeding 1 [1, 2].

When the calculations are evaluated, the device made with ZnO having a concentration of 2 wt.% CuPc stands out as the best diode because it exhibits the best electrical properties such as RR , n , and Φ_{Bo} . Table 2 lists the comparison of the electrical parameters of various hybrid heterojunctions at room temperature. As shown in the table, the Al/CuPc:ZnO/p-Si hybrid heterojunction fabricated in this study has similar ideality factor and barrier height compared to other p-n heterojunctions. On the other hand, it is observed that it has higher rectification ratio and shunt resistance and smaller series resistance than the reports of other studies.

Both R_s and R_{sh} are critical in the characterization of the diode, with a low R_s increasing the voltage across the diode and a high R_{sh} reducing the leakage current. Thus, R_s and R_{sh} have a significant influence

on the performance of the diode. The total R_s is the sum of the resistances from the leads used in the experimental measurements, the metal contact resistances and the resistances inherent in the semiconductor material. Consequently, R_s can cause severe inaccuracies in the computation of electrical properties, both in the dark and in the light, and in particular can lead to deviations from linearity in the $\ln I$ vs V plot. R_s and R_{sh} have been calculated for photodiodes with different CuPc doping levels using Ohm's law ($R_i = dV/dI$). Figure 5 depicts the resistance profiles dependent on voltage under both dark conditions and light intensity at 100 mW/cm². R_s and R_{sh} data for each sample are given in Table 2. R_s and R_{sh} measured values represent resistance levels found at strong forward and reverse bias circumstances.

The initial trend of the R_s values is to decrease, followed by an increasing trend as the doping concentration increases. This is explicable as; a higher concentration of CuPc in the films leads to an increased availability of additional conduction electrons, which causes the film resistance to decrease and consequently R_s to decrease, as is also observed in the Table 2. When the surface of a Si wafer is covered with an active layer of ZnO in CuPc doping, the uniformity of the active layer changes. As a result, the presence of CuPc contributes to a decrease in the series resistance of the device. On the other hand, variables such as the interlayer, its homogeneity, space charge injection and the presence of interface

Table 2 Comparison of electrical parameters

	I_o (A)	n	Φ_{Bo} (eV)	RR	R_s (kW)	R_{sh} (MW)	References
Al/ZnO/p-Si	3×10^{-9}	3.50	0.74	250	5.4		[20]
Au/ZnO/n-Si	1.37×10^{-10}	6.00	0.80	93	0.12		[21]
Au/ZnO/n-Si		1.21	0.61	3000	1.8		[22]
Al/ZnO/p-Si	2.32×10^{-7}	4.55	0.65	541	0.87	0.47	[35]
Al/CuPc/p-Si	–	2.38	0.71	350	43.5	–	[36]
p-CuPc/a-Si/n-Si	–	2.50	0.95	–	26	9.2	[27]
p-CuPc/a-Si/p-Si	–	5.70	0.93	–	28.6	3.7	[27]
Al/Au-CuPc /n-Si	–	1.64	0.72	–	254	–	[26]
Pd/Cu:p-ZnO/n-Si	4.57×10^{-8}	2.08	0.68	1190	–	–	[37]
Al/CuPc/n-Si	3×10^{-9}	3.91	0.59	1770	2.46	3	[38]
Au/ZnPc/Si		4.87	0.69	208	7.9		[39]
Al/Zn(II)Pc/p-Si	4.87×10^{-8}	4.06	0.74	6130	18.95		[40]
p-FePc/p-Si		4.07	1.10		159	132	[41]
Al/H ₃ BO ₃ (%1):ZnO/p-Si	5.99×10^{-10}	4.33	0.77	1660	0.55	0.91	[35]
Al/CuPc(%2):ZnO/p-Si	5.19×10^{-9}	4.01	0.75	9200	0.84	93	Present work

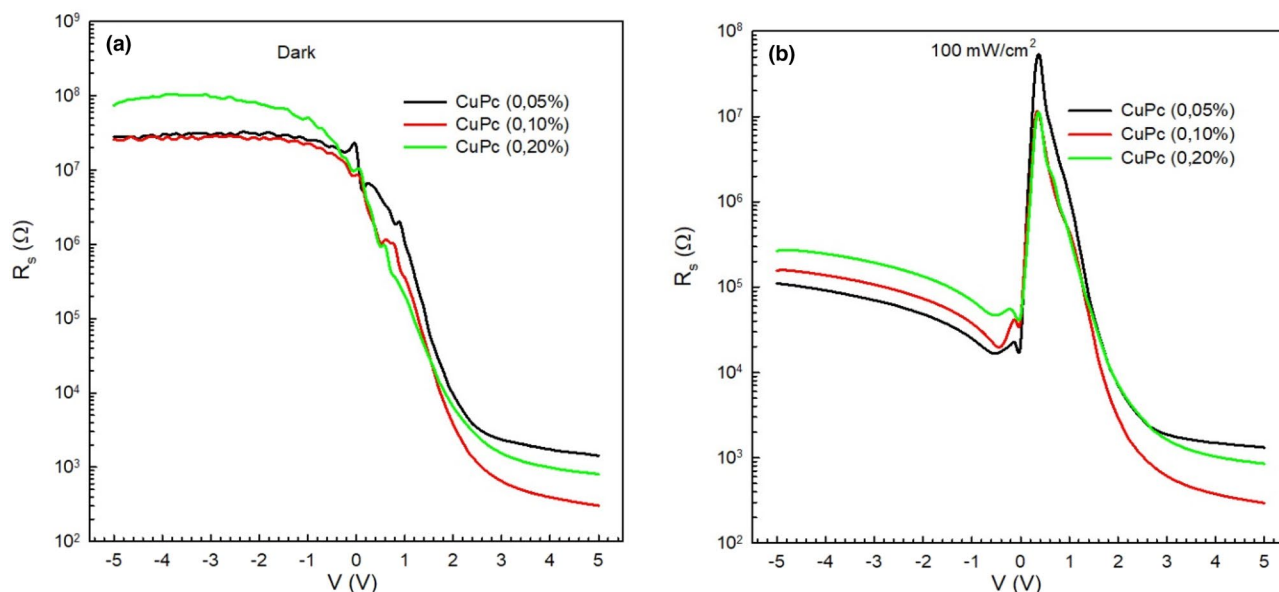


Fig. 5 The R_s - V characteristics for Al/CuPc:ZnO/p-Si photodiodes with different CuPc contents **a** for dark conditions **b** under an illumination intensity of 100 mW/cm^2

states or structural defects could explain the significant increase in R_s [42].

The presence of N_{ss} or that may have been formed during the fabrication process and may be located at energy levels within the band gap (E_g) of the semiconductor, particularly at the interface, is another critical device parameter that requires in-depth investigation. Several factors can influence the presence of surface traps including defects, unpaired interfacial bonds and oxygen vacancies [1, 2]. Both in the absence of light and in well-illuminated environments, these traps or structural inconsistencies might have a substantial impact on the device’s functionality under varying illumination conditions. These may act as centers for electrons to recombine, trapping and releasing electrons as a function of external factors such as electric fields, radiation and temperature fluctuations. The voltage-dependent ideality factor ($n(V)$) and the effective barrier height (Φ_e) are determined by means of the following equations [2]:

$$n(V) = \frac{q}{kT} \left[\frac{(V - IR_s)}{\ln(I/I_0)} \right] = 1 + \frac{\delta}{\epsilon_i} \left[\frac{\epsilon_s}{W_D} + qN_{ss}(V) \right] \quad (10)$$

$$\Phi_e = \Phi_{B_0} + \beta(V - IR_s) = \Phi_{B_0} + \left(1 - \frac{1}{n(V)} \right) (V - IR_s) \quad (11)$$

Here, β is the coefficient of effective BH voltage. From the I - V measurements, the energy density distribution of N_{ss} is derived using the following Card and Rhoderick formula [2];

$$N_{ss}(V) = \frac{1}{q} \left[\frac{\epsilon_i}{\delta} (n(V) - 1) - \frac{\epsilon_s}{W_D} \right] \quad (12)$$

“ δ ” interfacial layer thickness, “ W_D ” depletion layer width determined from the C^{-2} - V plot, and “ ϵ_i ” and “ ϵ_s ” interfacial layer permittivity. The energy position of the surface states (E_{ss}) in relation to the valence band (E_v) for p-type semiconductors and given as follows:

$$E_{ss} - E_v = q(\Phi_e - V) \quad (13)$$

The achieved findings are shown in Fig. 6a, b. These show visually how both light and the percentage of CuPc affect the surface states. Figure 6 shows, the plots depicting N_{ss} exhibit a pronounced exponential rise as one moves from the midpoint of the silicon bandgap toward the valence band edge (E_v).

3.2 Transient photocurrent, phot capacitance/ conductance features

Time-dependent transient photocurrent response technique was employed to evaluate the efficacy of electron–hole pair generation and to elucidate both the photoconduction mechanism and the stability of

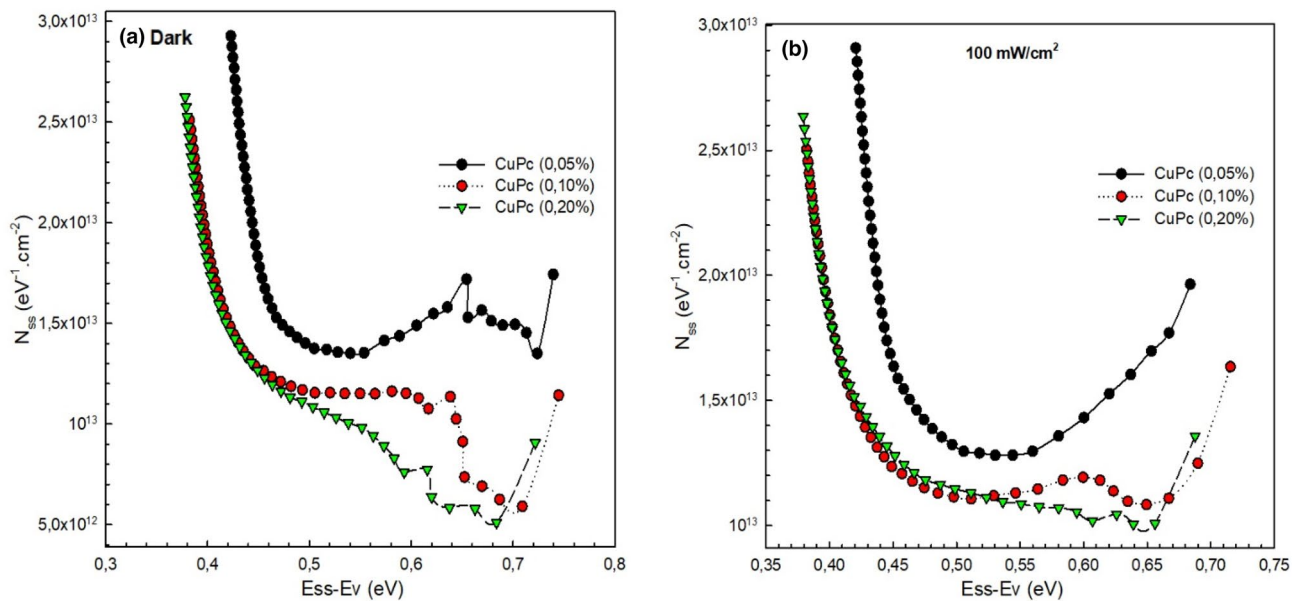


Fig. 6 The $N_{ss}-(E_{ss}-E_V)$ characteristics for Al/CuPc:ZnO/p-Si photodiodes with different CuPc contents **a** for dark conditions **b** under an illumination intensity of 100 mW/cm^2

photoresponse in Al/CuPc:ZnO/p-Si photodiodes. With an applied bias of -5 V , the illumination was alternately switched on and off at different intensity levels. Figures 7a–c show the evolution of the photocurrent in these photodiodes as a function of time. It is evident from these figures that as the illumination intensity increases, the photocurrent also rises. This is due to the increasing number of carriers generated by the incident light. These carriers contribute to the total current. After that, the current levels reach a point of saturation. As soon as the light source is switched off, the current returns to its initial value. Both of these situations could be explained by the fact that charge trapping takes place in the deep levels. The I_{on}/I_{off} rate was calculated from these figures at 1 and 9 s and 100 mW/cm^2 to be 980, 484 and 274 for S1, S2, and S3, respectively. The best photoresponse value is obtained for S1 and decreases with increasing CuPc content. Yasar et al. [43] growth Cu_2SnS_3 thin films with Triton-X100 surfactant by using sol–gel spin coating on the n-Si substrate and they found I_{on}/I_{off} rate as 347 under the light intensity of 100 mW/cm^2 . Demirbilek et al. [44]. calculated as 271.22 for co-doped n-Si/ZnO:Al 1%:Cd 2% photodiode under the light intensity of 100 mW/cm^2 . As a result, this indicates that the devices exhibit photoconductive behavior. This observed behavior is related to carrier trapping in deep impurity levels in the photodiode [19, 34, 45–48].

Graphical representations of the time-dependent measurements of the transient photocapacitance/conductance, for Al/CuPc:ZnO/p-Si photodiodes are also shown in Figs. 8a–c and 9a–c. These measurements have been carried out at a frequency of 10 kHz, with the intensity of the illumination varying in different conditions. When the light is switched on, both the photocapacitance and the photoconductance increase significantly as a result of the generation of charge carriers by the illumination. However, these parameters decrease and return to their initial values as soon as the illumination is switched off. On the other hand, these findings indicate that, the fabricated Al/CuPc:ZnO/p-Si photodiodes exhibit favorable behavior in terms of photocapacitance and photoconductance. Consequently, they have potential photocapacitor applications.

3.3 Capacitance/conductance-voltage features

In order for inspect a comparative analysis of the capacitance–voltage ($C-V$) and conductance–frequency ($G/\omega-V$) measurements for the photodiodes labelled S1, S2, and S3 at two different frequencies, 10 kHz and 1 MHz, Figs. 10 and 11 have plotted. These figures show the presence of notable areas within the $C-V$ and $G/\omega-V$ curves, such as inversion, depletion and accumulation. Applying an electric

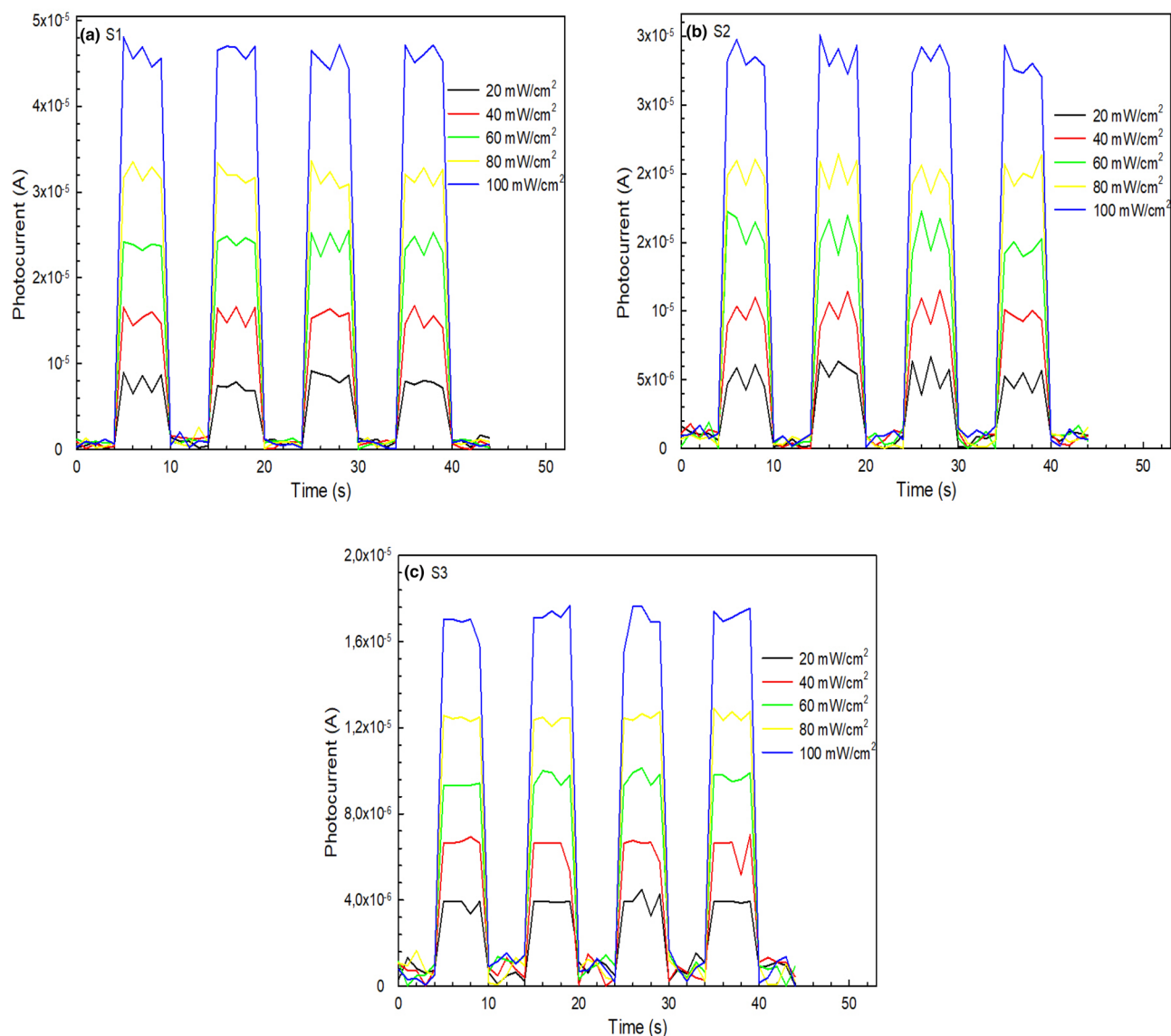


Fig. 7 Photocurrent-time curves for Al/CuPc:ZnO/p-Si photodiodes at -5 V

field has little effect on the diode's capacitance in the inversion region but causes significant capacitance changes in the accumulation region. It is also important to note that the C and G values at 10 kHz exceed those recorded at higher frequencies across the voltage region. The presence of interface states (N_{ss}) and their distribution in terms of spatial density within the silicon (Si) band gap are responsible for these increased levels of C and G with decreasing frequency. The interaction between the relaxation and lifetime of the interface states and the frequency of the applied ac signal causes the N_{ss} to follow the ac

signal, leading to the observed excess capacitance and conductance. Additionally, we observed that capacitance values changing with rising CuPc content, particularly at low frequencies. This increase can be ascribed to a distinctive distribution density of interface states [49–51].

Additional critical electrical parameters for SBDs, including diffusion potential or built-in potential (V_D), dopant concentration (for acceptor atoms) (N_A), depletion layer width (W_D), Fermi energy level (E_F) and Φ_B , were determined using the intercept and slope of C^{-2} - V curve at 1 MHz, employing the following relationships [1];

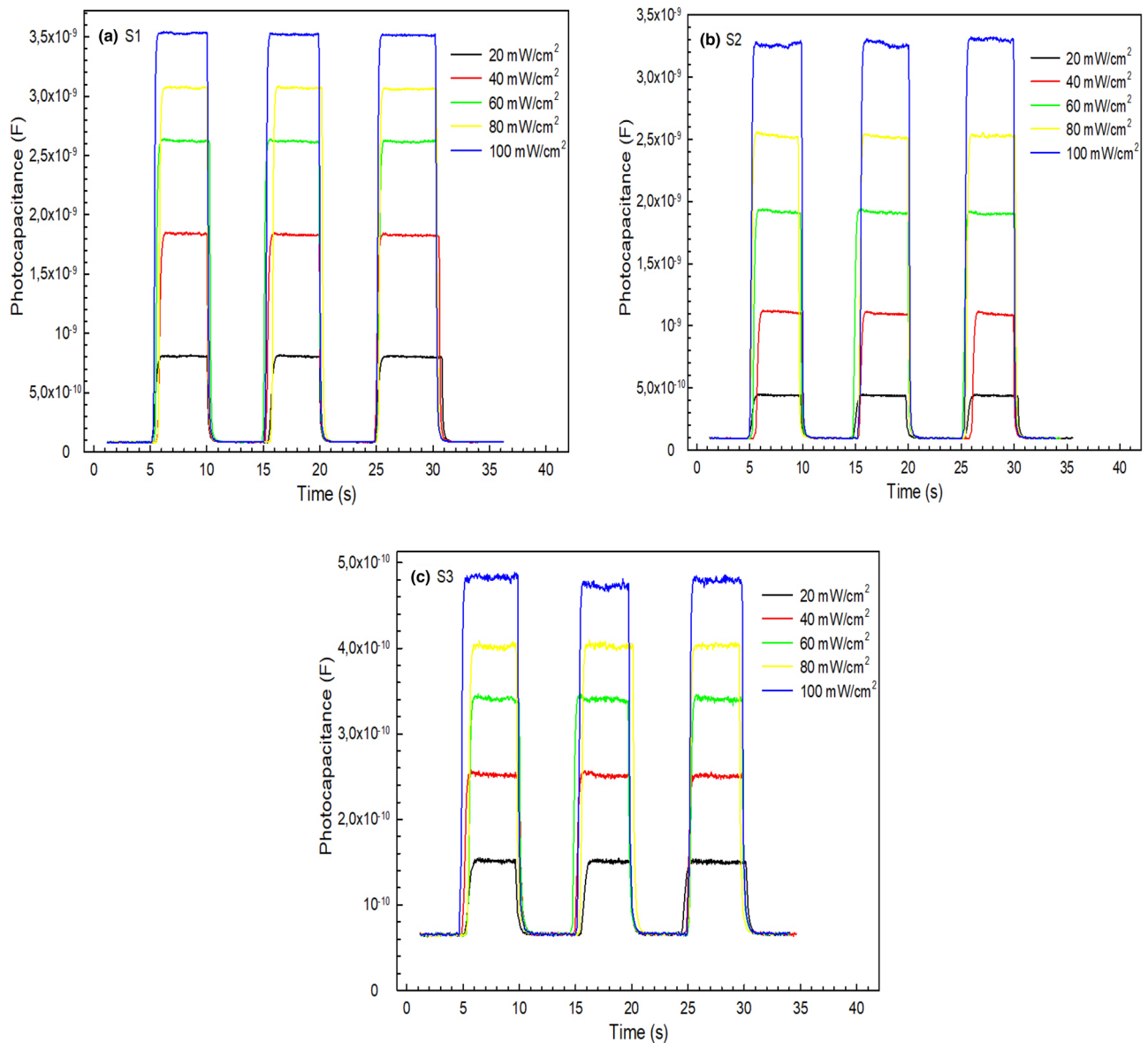


Fig. 8 Photocapacitance-time curves for Al/CuPc:ZnO/p-Si photodiodes

$$V_D = V_0 + \frac{kT}{q} \tag{14}$$

$$N_V = 4.82 \times 10^{15} T^{3/2} \left(\frac{m_h^*}{m_0} \right)^{3/2} \tag{17}$$

$$N_A = \frac{2}{q \epsilon_0 \epsilon_s A^2 \underbrace{\frac{d(1/C^{-2})}{dV}}_{\text{slope}(\tan \theta)}} \tag{15}$$

$$W_D = \sqrt{\frac{2 \epsilon_s \epsilon_0 V_D}{q N_A}} \tag{18}$$

$$E_F = \frac{kT}{q} \ln \left(\frac{N_V}{N_A} \right) \tag{16}$$

$$\Phi_B(C - V) = V_D + E_F \tag{19}$$

Table 3 shows the obtained experimental values. The increased value of Φ_B observed in the interfacial layer doped with 0.20% CuPc in ZnO is due to

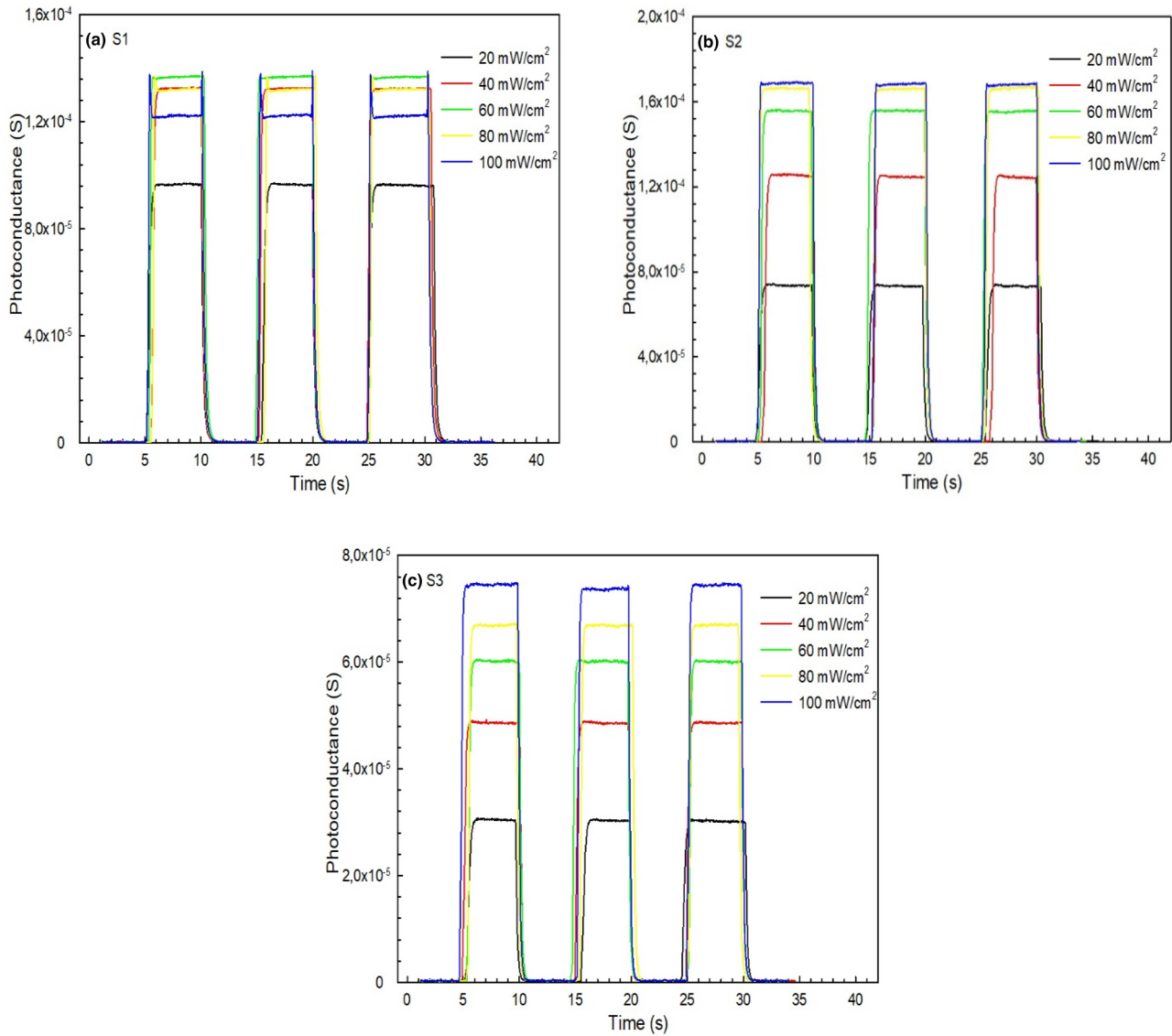


Fig. 9 Photoconductance-time curves for Al/CuPc:ZnO/p-Si photodiodes

the significant doping level, resulting in a significant increase in the intercept point.

Series resistance is another important electrical parameter because the interface's series resistance significantly affects the real capacitance and conductance, hence influencing the electrical characteristics. Based on the measured values of C_m and G_m/w at the strong accumulation region, the voltage-dependent plots of R_s for photodiodes S1, S2, and S3 were determined using the Eq. 13 known as Nicollian and Brews [52] formula;

$$R_s = \frac{G_m}{G_m^2 + (\omega C_m)^2} \tag{20}$$

In this equation, ω is angular frequency ($= 2\pi f$). In Fig. 12a, b, it can be clearly seen that the photodiodes show higher R_s values at low frequency (10 kHz), and the peaks observed from 10 kHz to 1 MHz are related to the reorganisation and rearrangement of N_{ss} due to relaxation times and spatial density distributions, which depend on the electric fields [31, 53].

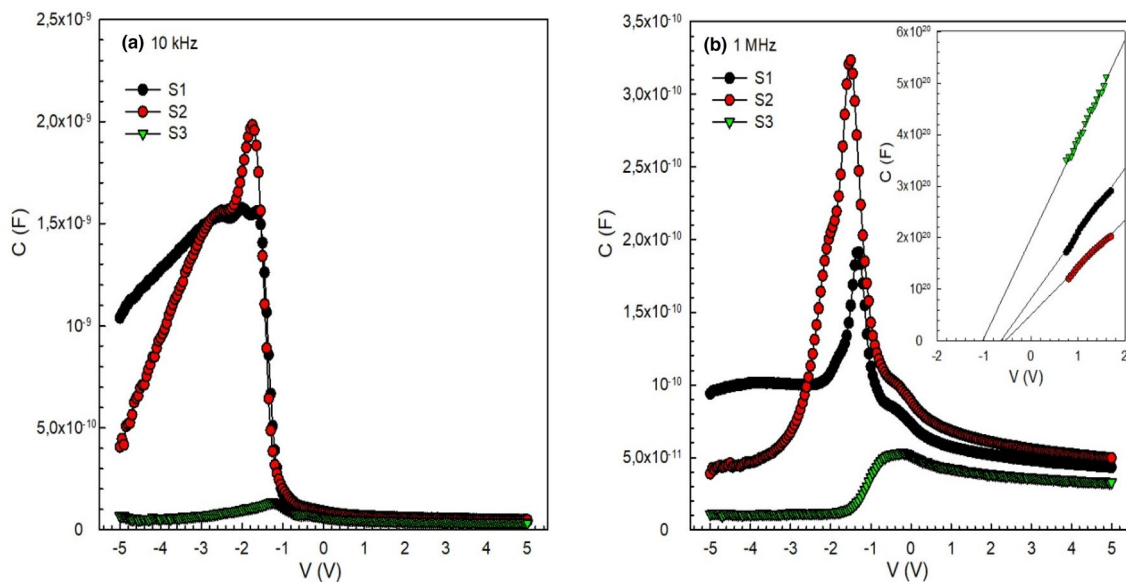


Fig. 10 The C–V plots of Al/CuPc:ZnO/p-Si photodiodes

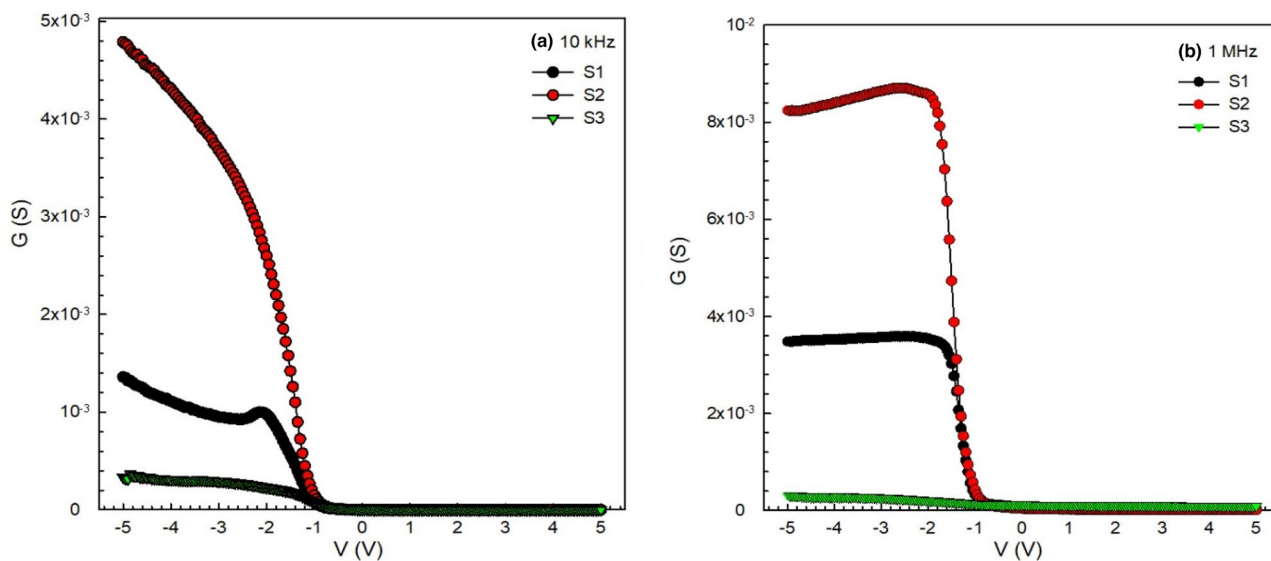


Fig. 11 The G–V plots of Al/CuPc:ZnO/p-Si photodiodes

Table 3 Main electrical parameters derived from the using C^{-2} -V plots

	V_0 (V)	N_A (cm^{-3}) ($\times 10^{15}$)	V_D (eV)	E_F (eV)	W_D (cm) ($\times 10^{-5}$)	Φ_B (eV)
S1	0.63	1.52	0.66	0.18	7.50	0.84
S2	0.52	2.08	0.55	0.17	5.85	0.72
S3	0.99	1.00	1.02	0.19	11.50	1.21

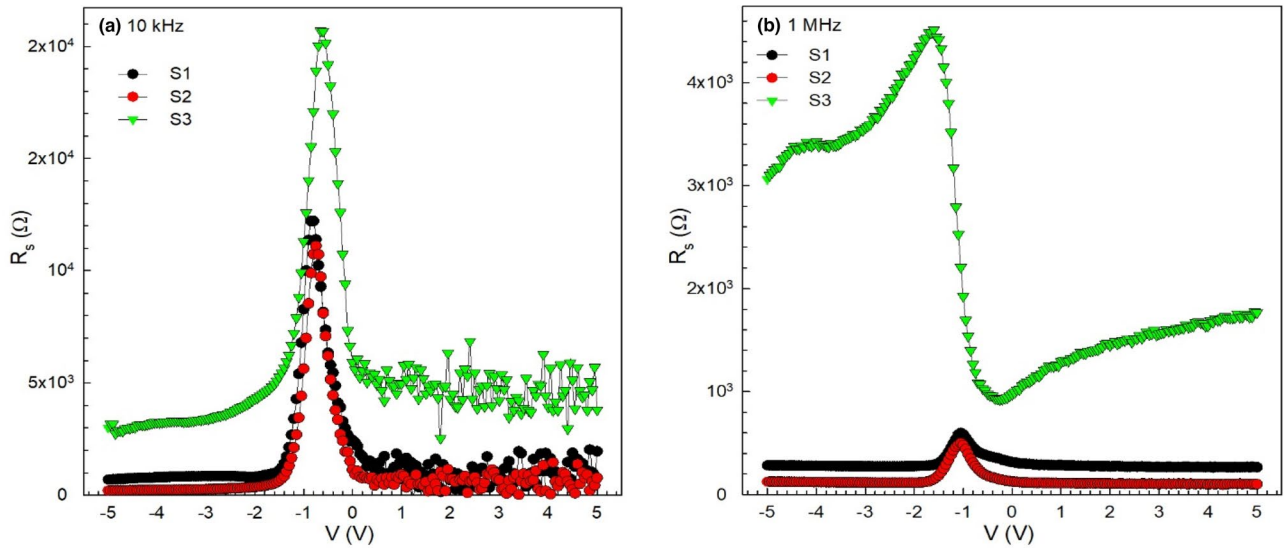


Fig. 12 The R_s plots for the Al/CuPc:ZnO/p-Si photodiodes

As noted above, there are indications that suggest R_s plays the most significant role in causing the less-than-ideal electrical characteristics of Schottky Barrier Diodes (SBDs). For the correct determination of the diode capacity and the diode conductance, the values C_m and G_m have been calculated again, considering the influence of R_s , as described by formulas 18, 19, and 20. The results are shown in Figs. 13a, and 4b for a frequency of 1 MHz.

$$C_c = \frac{[G_m^2 + (\omega C_m)^2] C_m}{a^2 + (\omega C_m)^2} \tag{21}$$

$$G_c = \frac{[G_m^2 + (\omega C_m)^2] a}{a^2 + (\omega C_m)^2}, \tag{22}$$

where “ a ” can be calculated as follows [52];

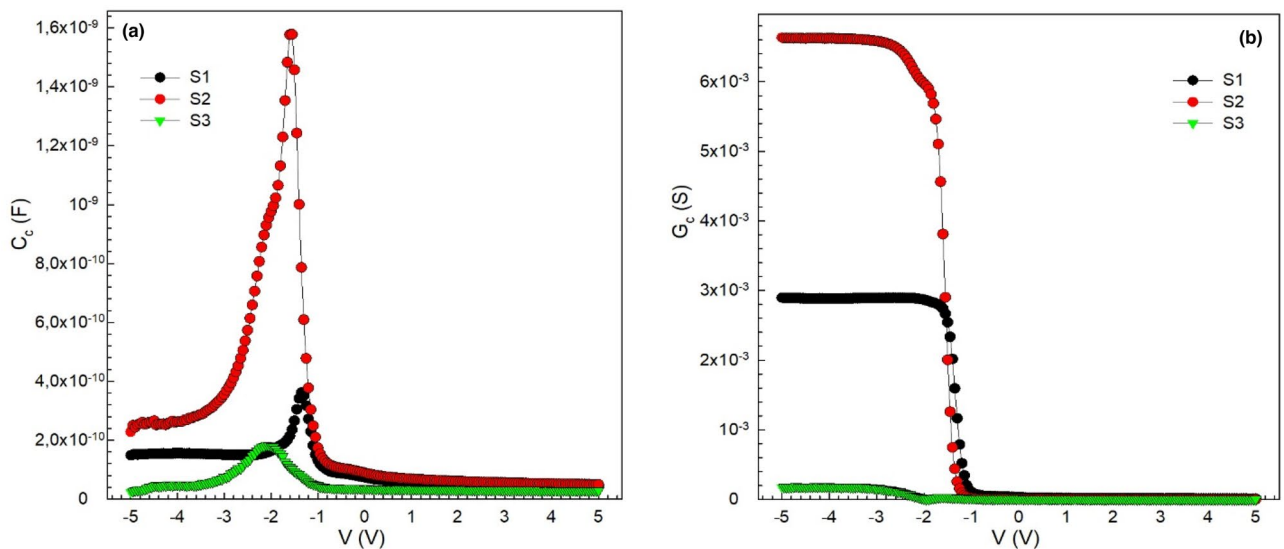


Fig. 13 Corrected **a** $C-V$ and **b** $G-V$ plots for the Al/CuPc:ZnO/p-Si photodiodes at 1 MHz

$$a = C_m - \left[G_m^2 + (\omega C_m)^2 \right] R_s, \quad (23)$$

As can be seen in Fig. 13, particularly in the accumulation region where the influence of R_s is attenuated, the corrected capacitance value (C_c) shows a significant increase and the corrected conductance value (G_c) shows a significant decrease compare to measured values. These findings lead to the inference that R_s plays a significant role in influencing the C and G measurements, particularly in both the depletion and accumulation zones, especially at higher frequencies. It is therefore essential to take this influence into account when calculating electrical and dielectric properties, especially [1, 52].

N_{ss} as a function of voltage was determined using a high-frequency/low-frequency (C_{HF} – C_{LF}) capacitance method [52]. This method, as outlined in Eq. 21 and illustrated visually in Fig. 14, quantifies N_{ss} by assessing capacitance to contribution to the total capacitance.

$$qAN_{ss} = \left[\left(\frac{1}{C_{LF}} - \frac{1}{C_{ox}} \right)^{-1} - \left(\frac{1}{C_{HF}} - \frac{1}{C_{ox}} \right)^{-1} \right] \quad (24)$$

In this equation, C_{LF} is the low-frequency capacitance, while C_{HF} is the high frequency capacitance. C_{ox} is the capacitance associated with the oxide/

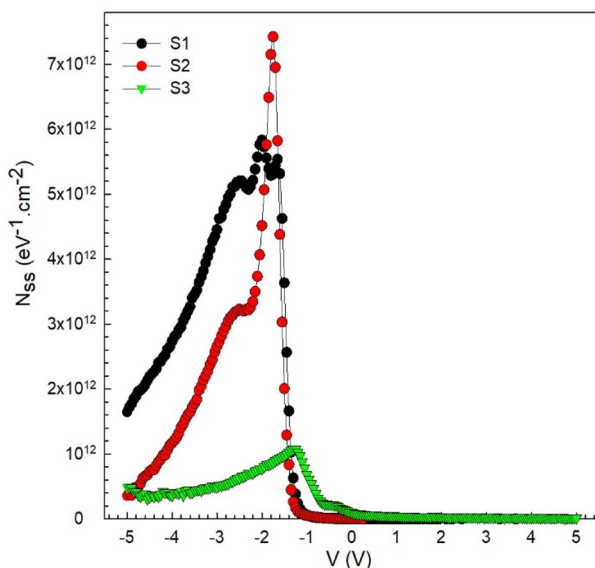


Fig. 14 The bias dependent N_{ss} curves for the Al/CuPc:ZnO/p-Si photodiodes

insulator layer/interface in the region of the accumulation. The variable ' q ' represents the electronic charge and ' A ' represents the area of the rectifier contact of the photodiodes.

Figure 1 illustrates that the maximum/peak values range from -2 V to -1 V for S1, S2, and S3, respectively. The spatial density distribution of the interface states between the CuPc:ZnO interfacial layer and the Si semiconductor is responsible for these findings [54]. The maximum recorded interface state density values were $5.76 \times 10^{12} \text{ eV}^{-1} \text{ cm}^{-2}$, $7.42 \times 10^{12} \text{ eV}^{-1} \text{ cm}^{-2}$, and $1.02 \times 10^{12} \text{ eV}^{-1} \text{ cm}^{-2}$ for S1, S2 and S3, respectively which are suitable for electronic devices [19, 24, 44].

4 Conclusion

The electrical characteristics of Al/CuPc:ZnO/p-Si photodiodes were determined by analyzing their I – V , C – V , and G – V characteristics under both dark and illuminated (0 – 100 mW cm^{-2}) conditions. The values of RR, I_{or} , n , Φ_{Bo} , and R_s were extracted from the I – V data, resulting in values of 1.9×10^4 , $0.11 \times 10^{-9} \text{ A}$, 8.26 , 0.73 eV , and 1490Ω for S1, 8.6×10^4 , $7.61 \times 10^{-9} \text{ A}$, 4.45 , 0.74 eV , and 319Ω for S2, and 9.2×10^4 , $5.19 \times 10^{-9} \text{ A}$, 4.01 , 0.75 eV , and 8360Ω for S3. These RR results highlight that structures exhibit favorable rectification behavior, The behavior of these structures in response to light was analyzed using the $I_{ph} = AP^m$ relationship, with values of m determined as 0.69 , 0.69 , and 0.66 for the respective diodes and this points to a linear photoconductivity mechanism in the diodes. On the other hand, the I_{on}/I_{off} rates were calculated as 980 , 484 , and 274 for S1, S2, and S3, respectively. Moreover, the LDR values calculated order of 14 which shows the obtained photodiodes using with image sensor applications. By examining the C – V and G – V data and taking into account the effect of interfacial conditions and R_s , it is clear that both capacitance and conductance have voltage and frequency sensitive. The results suggest that the concentration of CuPc doping has a significant effect on the electrical and optoelectronic properties of these diodes such as significantly reduces the values of N_{ss} and R_s , potentially making them suitable for use as photodiodes, sensors or detectors in optoelectronic applications.

Acknowledgements

This work is supported by Amasya University BAP research Project with FMB-BAP 19-0393 Number.

Author contributions

Gökhan Özel: Investigation, Visualization, Writing-review and editing. Selçuk Demirezen: Methodology, Investigation, Conceptualization, Data curation, Supervision, Validation, Writing—original draft.

Funding

Open access funding provided by the Scientific and Technological Research Council of Türkiye (TÜBİTAK). Funding was provided by Amasya Üniversitesi (FMB-BAP 19-0393).

Data availability

The datasets generated and/or analyzed during the current study are not publicly available due to that the data also form part of an ongoing study, but are available from the corresponding author on reasonable request.

Declarations

Conflict of interest The authors declare that they have no known competing financial interests or personal relationships that could have appeared to influence the work reported in this paper.

Ethical approval Hereby I consciously assure that for the manuscript the following is fulfilled: This material is the authors' own original work, which has not been previously published elsewhere. The paper is not currently being considered for publication elsewhere. The paper reflects the authors' own research and analysis in a truthful and complete manner. The paper properly credits the meaningful contributions of co-author and co-researcher. The results are appropriately placed in the context of prior and existing research. All sources used are properly disclosed (correct citation). Literally copying of text must be indicated as such using quo-

tation marks and giving proper reference. The author has been personally and actively involved in substantial work leading to the paper and will take public responsibility for its content.

Open Access This article is licensed under a Creative Commons Attribution 4.0 International License, which permits use, sharing, adaptation, distribution and reproduction in any medium or format, as long as you give appropriate credit to the original author(s) and the source, provide a link to the Creative Commons licence, and indicate if changes were made. The images or other third party material in this article are included in the article's Creative Commons licence, unless indicated otherwise in a credit line to the material. If material is not included in the article's Creative Commons licence and your intended use is not permitted by statutory regulation or exceeds the permitted use, you will need to obtain permission directly from the copyright holder. To view a copy of this licence, visit <http://creativecommons.org/licenses/by/4.0/>.

References

1. S.M. Sze, *Physics of Semiconductor Devices*, 2nd edn. (Wiley, New York, 1981)
2. E.H. Rhoderick, R.H. Williams, *Metal-Semiconductor Contacts*, 2nd edn. (Clarendon Press, Oxford, 1988)
3. E. Aldirmaz, *J. Mater. Sci.* **33**, 15023 (2022)
4. A. Eroğlu, S. Demirezen, Y. Azizian-Kaladaragh, Ş Altındal, *J. Mater. Sci.* **31**, 14466 (2020)
5. S. Demirezen, H.G. Çetinkaya, Ş Altındal, *SILICON* **14**, 8517 (2022)
6. E.E. Tanrikulu, S. Demirezen, Ş Altındal, İ Uslu, Altındal, İ. Uslu. *J. Mater. Sci.* **28**, 8844 (2017)
7. S. Kasap, P. Capper (eds.), *Springer Handbook of Electronic and Photonic Materials* (Springer International Publishing, Cham, 2017)
8. A. Kocuyigit, S. Aydoğan, Ü. Incekara, M. Yılmaz, *IEEE Sens. J.* **23**, 8184 (2023)
9. Ş Altındal, A.F. Özdemir, Ş Aydoğan, A. Türüt, *J. Mater. Sci.* **33**, 12210 (2022)
10. Ş Aydoğan, Ü. Incekara, A.R. Deniz, A. Türüt, *Microelectron. Eng.* **87**, 2525 (2010)
11. S. Cavdar, Y. Demirolmez, N. Turan, H. Koralay, N. Tuğluoğlu, L. Arda, *ECS J. Solid State Sci. Technol.* **11**, 025001 (2022)

12. O. Ongun, E. Taşcı, M. Emrullahoğlu, Ü. Akın, N. Tuğluoğlu, S. Eymur, J. Mater. Sci. **32**, 15707 (2021)
13. W.A. Farooq, E. Elgazzar, A. Dere, O. Dayan, Z. Serbetci, A. Karabulut, M. Atif, A. Hanif, J. Mater. Sci. **30**, 5516 (2019)
14. X. Liu, G. Sun, P. Chen, J. Liu, Z. Zhang, J. Li, H. Ma, B. Zhao, R. Wu, W. Dang, X. Yang, C. Dai, X. Tang, Z. Chen, L. Miao, X. Liu, B. Li, Y. Liu, X. Duan, Nano Res. **12**, 339 (2019)
15. A. Karabulut, A. Dere, A.G. Al-Sehemi, A.A. Al-Ghamdi, F. Yakuphanoglu, Mater. Sci. Semicond. Process. **134**, 106034 (2021)
16. Ü. Özgür, Ya. I. Alivov, C. Liu, A. Teke, M. A. Reshchikov, S. Doğan, V. Avrutin, S.-J. Cho, H. Morkoç, J. Appl. Phys. **98** (2005)
17. H.H. Gullu, D.E. Yildiz, A. Kocuyigit, M. Yıldırım, J. Alloys Compd. **827**, 154279 (2020)
18. B.A. Gozeh, A. Karabulut, M.M. Ameen, A. Yıldız, F. Yakuphanoglu, Surf. Rev. Lett. **27**, 1950173 (2020)
19. S. Demirezen, H.G. Çetinkaya, M. Kara, F. Yakuphanoglu, Ş Altındal, Sens. Actuators A **317**, 112449 (2021)
20. M. Benhaliliba, Int. J. Robot. Autom. Technol. **8**, 60 (2021)
21. L. Rajan, C. Periasamy, V. Sahula, Perspect. Sci. (Neth.) **8**, 66 (2016)
22. Ş Aydoğan, K. Çınar, H. Asıl, C. Coşkun, A. Türüt, J. Alloys Compd. **476**, 913 (2009)
23. M. Urbani, M.-E. Ragoussi, M.K. Nazeeruddin, T. Torres, Coord. Chem. Rev. **381**, 1 (2019)
24. M. Demiroglu, L. Sirka, E. Çalışkan, F. Biryan, K. Koran, A.O. Görgülü, F. Yakuphanoglu, J. Mol. Struct. **1219**, 128571 (2020)
25. X. Wang, J. Zheng, K. Qiao, J. Qu, C. Cao, Appl. Surf. Sci. **297**, 188 (2014)
26. P.R.S. Reddy, V. Janardhanam, K.-H. Shim, S.-N. Lee, A.A. Kumar, V.R. Reddy, C.J. Choi, Thin Solid Films **713**, 138343 (2020)
27. B. Tatar, D. Demiroğlu, M. Urgen, Microelectron. Eng. **108**, 150 (2013)
28. A.A. Al-Ghamdi, A. Dere, A. Tataroğlu, B. Arif, F. Yakuphanoglu, F. El-Tantawy, W.A. Farooq, J. Alloys Compd. **650**, 692 (2015)
29. E. Yükseltürk, O. Surucu, M. Terlemezoglu, M. Parlak, Ş Altındal, J. Mater. Sci. **32**, 21825 (2021)
30. M. Yıldırım, J. Alloys Compd. **773**, 890 (2019)
31. S. Demirezen, A.G. Al-Sehemi, A. Yüzer, M. Ince, A. Dere, A.A. Al-Ghamdi, F. Yakuphanoglu, J. Mater. Sci. **33**, 21011 (2022)
32. H. Ko, S. Park, H.J. Son, D.S. Chung, Chem. Mater. **32**, 3219 (2020)
33. Y. Zhao, C. Li, L. Shen, Chin. Phys. B **27**, 127806 (2018)
34. A. Tataroglu, K. Koran, E. Çaliskan, A.G. Al-Sehemi, A.O. Görgülü, A. Al-Ghamdi, F. Yakuphanoglu, SILICON **11**, 1275 (2019)
35. A.G. Al-Sehemi, A. Tataroglu, A. Karabulut, A. Dere, A.A. Al-Ghamdi, F. Yakuphanoglu, JOM **75**, 3587 (2023)
36. F. Yakuphanoglu, Sol. Energy Mater. Sol. Cells **91**, 1182 (2007)
37. L. Agarwal, S. Tripathi, P. Chakrabarti, J. Semicond. **38**, 104002 (2017)
38. E. Elgazzar, Mater. Res. Express **7**, 095102 (2020)
39. M. Benhaliliba, I. Missoum, S. Ozcelik, T. Asar, Optik (Stuttg.) **206**, 163629 (2020)
40. A.G. Al-Sehemi, K. Ocakoglu, M. Ince, A. Karabulut, A. Tataroğlu, A. Dere, A.A. Al-Ghamdi, F. Yakuphanoglu, Polym. Bull. **81**(5), 4351–4368 (2023)
41. B. Tatar, D. Demiroğlu, Mater. Sci. Semicond. Process. **31**, 644 (2015)
42. B. Akin, J. Farazin, Ş Altındal, Y. Azizian-Kalandaragh, J. Mater. Sci. **33**, 21963 (2022)
43. S. Yaşar, S. Kahraman, S. Çetinkaya, İ Bilican, J. Alloys Compd. **618**, 217 (2015)
44. N. Demirbilek, F. Yakuphanoglu, M. Kaya, Prot. Met. Phys. Chem. Surf. **57**, 488 (2021)
45. W. Khan, S.-D. Kim, Mater. Sci. Semicond. Process. **66**, 232 (2017)
46. A. Mekki, R.O. Ocaya, A. Dere, A.A. Al-Ghamdi, K. Har-rabi, F. Yakuphanoglu, Synth. Met. **213**, 47 (2016)
47. J. Moore, C. Thompson, Sensors **13**, 9921 (2013)
48. O. Çiçek, H.U. Tecimer, S.O. Tan, H. Tecimer, Ş Altındal, İ Uslu, Composites B **98**, 260 (2016)
49. A. Tataroğlu, A.A. Al-Ghamdi, F. El-Tantawy, W.A. Farooq, F. Yakuphanoglu, Appl. Phys. A **122**, 1 (2016)
50. E.E. Tanrikulu, S. Demirezen, Ş Altındal, İ Uslu, J. Mater. Sci. **29**, 2890 (2018)
51. S. Demirezen, I. Orak, Y. Azizian-Kalandaragh, and Altındal. J. Mater. Sci. **28**, 12967 (2017)
52. E. H. Nicollian and J. R. Brews, *Metal Oxide Semiconductor (MOS) Physics and Technology* (New York, 1982).
53. S. Demirezen, A. Dere, H.G. Çetinkaya, A.G. Al-Sehemi, A.A. Al-Ghamdi, F. Yakuphanoglu, Phys. Scr. **98**, 115916 (2023)
54. F.Z. Acar, A. Buyukbas-Ulusan, A. Tataroglu, J. Mater. Sci. **29**, 12553 (2018)

Publisher's Note Springer Nature remains neutral with regard to jurisdictional claims in published maps and institutional affiliations.